Microwave Assisted Zinc Sulphide Quantum Dots for Energy Device Applications

Aman Rai[1], Peeyush Phogat[1], Shreya[1], Ranjana Jha[1], and Sukhvir Singh [1]*

[1]Research Lab for Energy Systems, Department of Physics, Netaji Subhas University of Technology, Delhi, India

Abstract.

Zinc sulfide (ZnS) quantum dots (QDs) have received a lot of attention because of their potential usage in solar cell applications. The present work illustrates a straightforward green synthesis route for ZnS QDs, which is both cost-effective and environmentally friendly. The phase identification of the synthesized material was performed through the X-ray diffraction technique which revealed the presence of single-phase zinc sulfide. The crystallite size was calculated through various techniques such as Debye Scherrer's, Williamson Hall and Size-Strain plot revealing quantum confinement effects. High-resolution transmission electron microscope (HR-TEM) revealed the presence of quantum dots within the quantum size range and demonstrated excellent quantum yield. However, the decrease in the particle size has increased the band gap for ZnS QDs to 3.4 eV with a refractive index of 2.29. The polycrystalline character of the as-synthesized ZnS was shown by the selected area electron diffraction (SAED) pattern of the corresponding TEM images. Morphological analysis, carried out via field emission scanning electron microscopy (FESEM), unveiled the existence of zinc sulfide quantum dots agglomerates. Elemental composition analysis was performed using energy dispersive spectroscopy (EDS) as an attachment to FESEM, which confirmed the existence only of zinc and sulphur.

Keywords: Zinc Sulfide, reduced band gap, Microwave, Solar cell

1 Introduction

Nanoparticles due to their unique characteristics and versatility, have gained significant importance in different fields. Among these, Quantum dots (QDs) have shown outstanding efficacy in photonic devices, attracting significant interest in a variety of applications. QDs offer several benefits over standard organic fluorophores,
Such as having high fluorescence intensity, broad absorption coefficients, narrow emission spectra, size-dependent emission, and strong photostability[1]. Over the years, efforts have been made for the

* Corresponding author: peeyush.phogat@gmail.com

synthesis of high fluorescent QDs. The quantum confinement effect further amplifies these characteristics, resulting in narrow emission spectra and a wide range of excitation wavelengths[2]. Such characteristics attracted significant interest in technical applications such as biological fluorescence and imaging[3]. These nanoparticles have also been used in wastewater treatment as well as water-splitting photocatalytic degradation and disinfection methods.

ZnS is a wide band gap II–VI semiconductor nanomaterial. Over the years many synthesis routes have been taken to prepare zinc sulfide QDs which include the hydrothermal method, co-precipitation method, microwave-assisted method, and many more the quantum confinement effect limits the spatial mobility of the exciton within a particle[4]–[6]. This confinement causes the formation of discrete energy levels, also known as energy sub-bands, with greater energy band gaps. As a result, when compared to the analogous bulk materials, these altered energy characteristics have apparent impacts on the electrical and optical properties. The structure and morphology of ZnS QDs are certainly the most important in achieving enhanced photoelectrical characteristics. Over several years, the synthesis of ZnS quantum dots has been the focus of research, with attempts made to improve the material's optical and structural features[7]–[10].

The present study accentuates the synthesis of zinc sulfide QDs by microwave-assisted method. The novelty of the presented work lies in microwave synthesis, where particle size reduction has been seen. Furthermore, the given work focuses on low-cost green synthesis. The X-ray diffraction pattern (XRD) was used to study structural information. UV-Vis spectroscopy was used to analyse the sample's optical and electrical properties. A transmission electron microscope (HR-TEM) and a field emission scanning electron microscope (FE-SEM) were used for microstructural and morphological study.

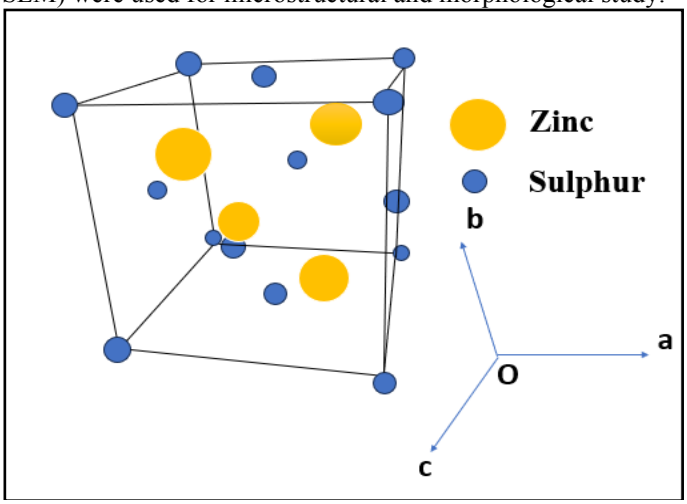

Fig.1 3D model of cubic ZnS.

2 Experimental Information

2.1 Chemical Used

Distilled water (DI) of near 5 mega-Ohm resistance and absolute alcohol was used for cleaning and washing purposes. All the solutions were prepared in DI water if not specified otherwise. All other chemicals used in synthesis are listed in Table 1.

Table 1 Chemicals Used

Chemicals Name	Company
Zinc oxide [ZnO]	M/s THOMAS BAKER
Sodium Sulfide [Na_2S]	M/s THOMAS BAKER

2.2 Synthesis

A 0.15 M colloidal solution of zinc oxide was synthesized by dispersing zinc oxide nanoparticles of average particle size of 30nm into 80 ml DI. The solution was then given microwave heating for 4 hours at 60^o C along with ultraviolet (UV) radiation and ultrasonic vibrations. In the meantime, 0.17 M of sodium sulphide was prepared in 70 ml DI and was stirred on a magnetic stirrer for 30 minutes. After 30 minutes sodium sulfide solution was added to the zinc oxide solution through a burette as slowly as possible. After four hours of agitation, the mixture was allowed to cool naturally in a room temperature of room temperature. Following that, the sample was centrifuged and washed with a water and ethanol to remove any probable impurities. Following that, the sample was heated in a vacuum oven to dry it, resulting in the production of a powdered sample. However, there are drawbacks associated with microwave synthesis. One such limitation is the nature of microwave heating, which can result in temperature fluctuations within the reaction container. Consequently, the size distribution of ZnS quantum dots (QDs) may be wider compared to heating techniques. Additionally, the quick heating process, in microwaves can cause nucleation and growth rates posing challenges in achieving precise control over the final size of the QDs. On the hand slower heating enables more regulated growth and enhances uniformity in size.

3 Result and Discussion

3.1 Characterization Details

The fine powdered of synthesized sample was analyzed using an X-Ray Diffractometer, make: Rigaku, model: smart lab 3KW X-Ray Diffractometer. Copper (Cu) Kα-radiation (λ=1.5406A^o) was used to record the x-ray diffraction pattern. FESEM (model:7610FPlus, make:

JEOL) with EDS as an attachment was used for the morphological and elemental compositional analysis. SHIMADZU UV-2600i Uv-Vis spectrometer was used to record the optical response of the as-synthesized material. The TEM images were taken by TECNAI(HR-TEM) operated at 200 KV.

3.2 X-ray Diffraction

The X-ray diffraction pattern for synthesized zinc sulfide was recorded over the range of 5^0 to 90^0 for $2\theta(^0)$ as shown in Fig-2. The obtained XRD spectra was then analysed and peaks for zinc sulphide were cross-referred with ***JCPDS file 98-007-7082*** showing a good match with single phase ZnS with cubic crystal system. The peaks were identified and marked with Miller indices (hkl) of (111), (002), (022), (113), (222), (004), (133), (024), and (244) shown in the figure. The as-synthesised ZnS X-ray pattern indicates a single-phase with space group F-43 m and space group number 216 which depicts that the synthesized zinc sulfide has FCC structure and symmetry along the axis rotation mirror plane and is centrosymmetric. Sharp and distinct peaks of zinc sulphide depicted a high crystalline nature.

The sample shows a cubic crystal structure for which the lattice parameter is given by equation-1 as given below ,

$$\frac{1}{d^2} = \frac{h^2}{a^2} + \frac{k^2}{b^2} + \frac{l^2}{c^2} \quad \text{.....(1)}$$

Here interplanar spacing is denoted by d, while the Miller indices are denoted by h,k,l. and for cubic structures, it is a well-known fact that a=b=c and α=β=γ. Table 2 presents the comparison of calculated lattice parameters and standard values from the JCPDS file.

Table2. Lattice Parameters

Parameters	As synthesized ZnS	ZnS in JCPDS file: *00-001-1047*
a (Å)	5.397	5.4090
b(Å)	5.397	5.4090
C(Å)	5.397	5.4090

3.3 Lattice Parameters, Crystallite Size and Strain

Crystallite size of a material is a significant parameter in material science which provides information about material characterization, Grain size distribution, mechanical properties, and optical properties. The crystallite size was determined using the widely known Debye-Scherrer formula given in equation 2 as[11],

$$D = \frac{K\lambda}{\beta Cos\theta} \quad \text{..... (2)}$$

In this equation, D denotes the crystal grain size (crystallite size), K is a constant of 0.9 referred to as the Scherrer constant λ is the wavelength of the x-ray source given by 0.154 nm, β is full with at half of the maxima (FWHM), and θ is half of the peak positions in the XRD pattern. The value of crystallite size applying Scherer's formula was found to be 14

nm, which was near the quantum confinement region, indicating that there were quantum electronic states and that they were constrained. Debye-Scherrer's analysis was predicated on the notion that the material is devoid of any strain and crystallite is spherical. However, that is not the case here.

The observed deviation in lattice parameters from their standard values indicates the existence of microstructural strain within the materials (as shown in Table 1). The strain was identified using a well-known method called the Williamson Hall plot. The broadening of XRD is attributed to strain and crystallite size, according to the Williamson-Hall plot (W-H plot). The W-H equation has the following formula[12] ,

$$\beta_T Cos\theta = (\varepsilon \times 4Sin\theta) + \frac{K\lambda}{D} \quad \ldots\ldots\ldots(3)$$

Where is ϵ strain, D refers to crystal grain size (crystallite size), K is a constant of 0.9 known as the Scherrer constant, and λ is the wavelength of the x-ray source, which is supplied by 0.154 nm. β is FWHM, or full width at half maximum, and θ is the half position of the XRD pattern also included in equation 3. Visualizing the graph of the 4Sinθ against Cosθ relation. The strain calculated through the W-H plot provides a negative strain or compression, with a crystallite size of 10 nm.

As the Williamson-Hall plot assumes stain in a material isisotropic.In reality,materials often have anisotropic strain which can make results less accurate therefore Size Strain(S-S) approach was also taken for the calculation of crystallite size and strain by using eq as[13],

$$(d\beta Cos\theta)^2 = \frac{K\lambda}{D} + (d^2\beta Cos\theta) + \frac{\varepsilon^2}{4} \quad \ldots\ldots\ldots\ldots (4)$$

Here, where ε is strain, D is related to crystal grain size (crystallite size), K is a constant of 0.9 known as the Scherrer constant, and λ is the wavelength of the x-ray source, which is given by 0.154 nm. β is FWHM, or full width at half maximum, and θ is half position of the XRD pattern

calculated values were found to be 10.2 nm and 0.00147 respectively, comparing the value of slope depicted in figure-3(a&b) reveals the micro strain to be 0.0027 by Williamson hall plot and 0.00147 by Size Strain plot. Due to the negative strain present, the material displays compression. Table 3 presents all the values calculated from the Debye-Scherrer equation-H plot and Size-Strain plot.

Table3. Crystallite Size and strain

Parameters	**Debye Scherrer**	**Williamson Hall plot**	**Size Strain Plot**
Size	14 nm	10 nm	10 nm
Strain	-	0.0027	0.00147

Dislocation is described as a flaw and imperfection in the crystal structure caused by atom displacement from their ideal lattice positions. Dislocation density is the number of dislocations per unit volume and was derived using the equation.

$$\delta = \frac{1}{D^2} \quad \ldots\ldots\ldots\ldots(5)$$

Where D is crystallite size and δ is dislocation density which was found to be 0.00368201.

A stacking fault is a form of crystallographic defect that develops when the usual stacking sequence is disrupted, which can occur during atom movement. Which is provided by,

$$\sigma = \frac{2\pi^2}{45(tan\theta)^{1/2}} \times \beta \qquad \text{.....(6)}$$

Where σ sacking fault,θ is peak position, β is full width half maxima. The stacking fault is found to be 0.224.

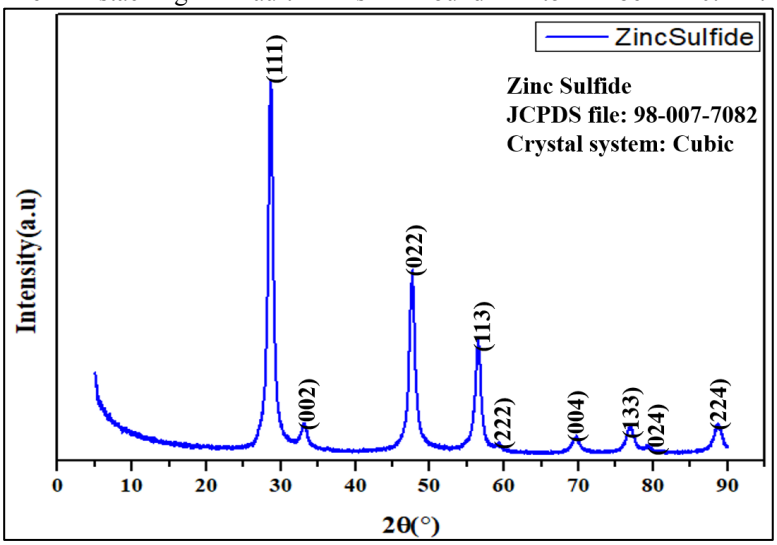

Fig.2 XRD pattern for Cubic Zinc Sulfide

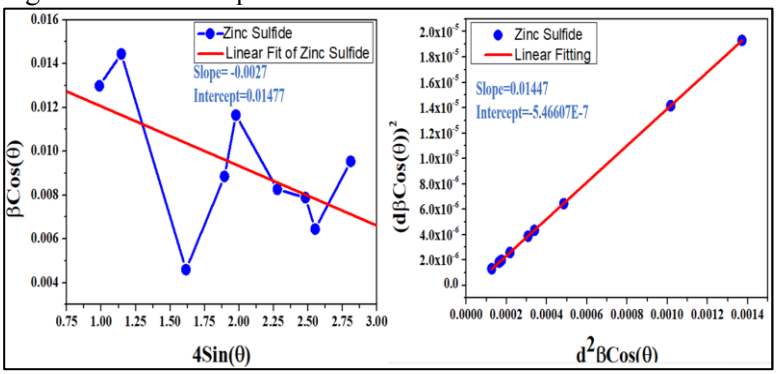

Fig.3.**(a)** Williamson Hall for Cubic ZnS. **(b)**Size Strain plot for cubic ZnS

3.4 UV-Spectroscopy

The UV-Vis spectra of as synthesized zinc sulfide was recorded in the wavelength range of 190 nm to 850 nm. The as-synthesized zinc sulfide showed absorption in the UV region only, which indicates that zinc sulfide has future applications which can impact the efficiency and performance of solar cells. UV absorption implies an increased capacity of photovoltaic materials to capture a broader range of sunlight and achieve more efficient energy conversion. In uv spectrum [Fig.3] highest absorbance peak is identified at 324 nm .

Size dependent band gap in QDs is a result of quantum effects. Smaller particles have larger band gap and vice versa. this unique behaviour of QDs allows precise control over band gap .Tauc plot shown in Fig.4 was obtained from further examination of absorption data and using beer lambert's principle which is given as[14],

$$\alpha h\upsilon = A[h\upsilon - E_g]^{\frac{1}{n}} \quad \ldots\ldots\ldots (7)$$

Where A = Absorbance(a.u); α= Molecular extinction coefficient ; h =Plank's constant ; υ=Frequency ; E_g= direct band gap ; n=1/2(direct band gap),2 (indirect band gap). For Zns (direct band gap) n=1/2.Extrapolation of plotted graph was done by linear fitting the data points to get the band gap value of 3.4 eV. The 3.4 eV band gap of ZnS allows it to efficiently absorb UV radiation in the shorter wavelength range, making it a valuable choice for applications that require sensitivity to UV light. Standard bandgap of bulk zinc sulfide is 3.68 eV. The refractive index plays an important role in the solar cell application of material. The refractive index can affect how efficiently light interacts with the layer of solar cell. When the refractive indices of the material and the medium are matched, more light can penetrate the medium and reach the absorbing layer, increasing the efficiency of solar cells. To determine the refractive index of the synthesized samples equation (5) has been taken into consideration[15],

$$\frac{n^2-1}{n^2+2} = 1 - \sqrt{\frac{E_g}{20}} \quad \ldots\ldots\ldots (8)$$

Where n represents the refractive index, while Eg signifies the direct band gap of zinc sulfide of 3.4 eV. The calculated refractive index from the 3.4 eV band gap came to be 2.29 which is relatively high indicating that the Synthesized sample is a strong optical medium and can significantly alter the path of light. High refractive indices are often associated with materials that are transparent and have optical properties useful for various optical applications.

HOMO represents the molecular orbit with the highest energy that contains electrons. When at ground state HOMO is the highest energy that an electron can stay at .LUMO can be described as the lowest energy in a molecule that does not contain any electrons. Calculation of HOMO(Valance band) and LUMO(Conduction band) band gap was done by equation below.

$$E_{VB} = \chi + E_e + 0.5 * E_g \quad \ldots\ldots\ldots\ldots (9)$$

$$E_{CB} = E_{VB} + E_g \quad \ldots\ldots\ldots\ldots\ldots (10)$$

Where χ is called absolute electronegativity which has a value of 5.26 eV for Zinc sulfide E_e is the free electron energy on the hydrogen scale, E_{VB} and E_{CB} are the energy of the valance band and conduction band respectively and E_g is band gap of Synthesized sample. Calculated energies of valance and conduction band came out to be 2.46 eV and 5.86 eV respectively. Band gap of 3.4 eV depicts that such material falls under the category of wide range bandgap material. The wide band gap allows this material to significantly absorb and emit high- energy radiation in ultra violet (UV) region. wide band gap of materials are beneficial in photovoltaic and solar cells where they capture high energy photons efficiently.

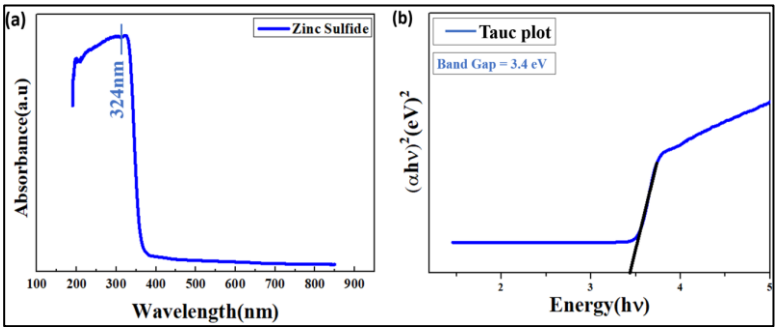

Fig.4.(a) Absorption spectra for ZnS,(b) Tauc plot spectra for ZnS.

3.5 FESEM

The morphological analysis of synthesized zinc sulfide was conducted using a High-Resolution Field Emission Scanning Electron Microscope(FE-SEM) equipped with Energy Dispersive Spectroscopy (EDX) (model-7610F plus, make-JEOL). As shown in Figure 4(a) and EDX spectrum in Fig.4(b) SEM images of Zns at high resolution and magnification depict that particles are in quantum confinement range which are aggregated due to high surface energy. While the materials were being synthesized, an EDX pattern was captured to confirm the elements present, and it showed the presence of high-intensity peaks due to Zn and S.

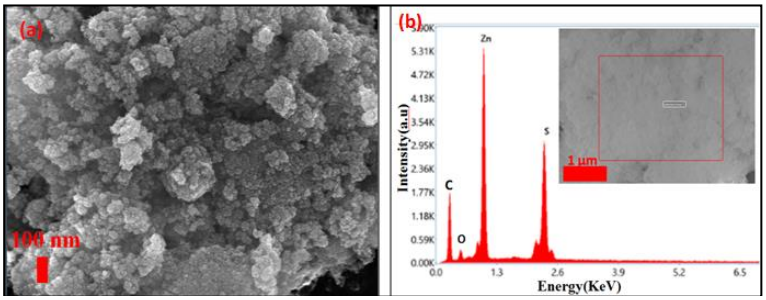

Fig.5**(a)** shows SEM image of ZnS taken at various magnifications. **(b)** EDX spectra of selected area for ZnS

3.6 HR-TEM

In this study, transmission electron microscopy (TEM) analysis was employed to visually assess the size, morphology, and dispersion characteristics of the as-prepared nanoparticles. As depicted in Figure 6(a), the TEM images reveal nanoparticles characterized by a nano-scaled size, spherical morphology, and a uniform spatial distribution. The average particle diameter is estimated to be approximately 15.8 nanometers. which is in agreement with the XRD results. The results are noteworthy, however, because a percentage of total particles had a diameter larger than 15 nm. Furthermore, large particles that appear to be the result of aggregation of Quantum Dots(QDs) are noticeable in Fig.6.These particles may only appear at rather high QD concentrations. Figure 6(b) demonstrates the corresponding area of the material's

selected area electron diffraction (SEAD) pattern and depicts the peak with hkl values of (111),(002), and (022)[16].

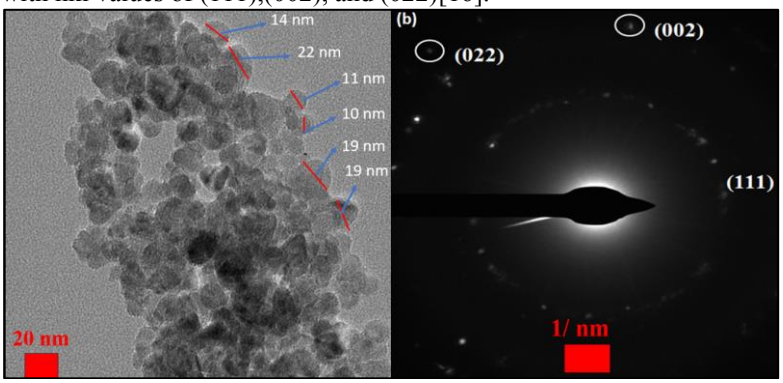

Fig.6**(a).** HR-TEM images of synthesized ZnS. (b) SEAD pattern of ZnS.

4 Conclusion

The current work is concentrated on the synthesis of ZnS with a reduced band gap. The ZnS was produced by conventional microwave synthesis. Structural study shows the presence of both zinc and sulfur. Scherer's formula determined the crystallite size to be 14 nm, which is within to the quantum confinement area. The W-H plot was used to calculate a negative strain associated with a crystallite size of 10 nm. In addition, dislocation density and stacking fault calculations were carried out. Band gap and refractive index ZnS were found to be 3.4eV and 2.29 respectively. SEM images show ZnS particles aggregated due to increased surface energy in the quantum confinement range. The EDX pattern indicates the elements by exhibiting high-intensity peaks caused by Zn and S. The transmission electron microscopy (TEM) analysis revealed nanoparticles with nano-scaled size, spherical morphology, and uniform distribution. The average particle diameter was 15.8 nanometers, with a percentage bigger than 15 nm. Large particles aggregating Quantum Dots occurred in great numbers.

References

[1] E. K. Goharshadi, S. H. Sajjadi, R. Mehrkhah, and P. Nancarrow, “Sonochemical synthesis and measurement of optical properties of zinc sulfide quantum dots,” *Chemical Engineering Journal*, vol. 209, pp. 113–117, Oct. 2012, doi: 10.1016/J.CEJ.2012.07.131.

[2] E. K. Goharshadi, R. Mehrkhah, and P. Nancarrow, “Synthesis, characterization, and measurement of structural, optical, and phtotoluminescent properties of zinc sulfide quantum dots,” *Mater Sci Semicond Process*, vol. 16, no. 2, pp. 356–362, Apr. 2013, doi: 10.1016/J.MSSP.2012.09.012.

[3] K. T. Al-Rasoul, I. M. Ibrahim, I. M. Ali, and R. M. Al-Haddad, “Synthesis, Structure And Characterization Of Zns Qds And Using It In Photocatalytic Reaction,” *INTERNATIONAL JOURNAL OF SCIENTIFIC & TECHNOLOGY*

RESEARCH, vol. 3, no. 5, 2014, Accessed: Dec. 05, 2023. [Online]. Available: www.ijstr.org

[4] M. Madkour *et al.*, "Nano-heterostructured photo-stable $Cd_xZn_{1\&\#x2212;x}S$ heterojunction as a non-photocorrosive visible light active photocatalyst," *Optical Materials Express, Vol. 6, Issue 9, pp. 2857-2870*, vol. 6, no. 9, pp. 2857–2870, Sep. 2016, doi: 10.1364/OME.6.002857.

[5] C. Ippen *et al.*, "ZnSe/ZnS quantum dots as emitting material in blue QD-LEDs with narrow emission peak and wavelength tunability," *Org Electron*, vol. 15, no. 1, pp. 126–131, Jan. 2014, doi: 10.1016/J.ORGEL.2013.11.003.

[6] W. Zhang *et al.*, "InP/ZnS/ZnS Core/Shell Blue Quantum Dots for Efficient Light-Emitting Diodes," *Adv Funct Mater*, vol. 30, no. 49, p. 2005303, Dec. 2020, doi: 10.1002/ADFM.202005303.

[7] H. Kumar, A. Kumari, and R. R. Singh, "Tunable narrow emission in ZnS/CdS/ZnS quantum well structures prepared by aqueous route," *Opt Mater (Amst)*, vol. 69, pp. 23–29, Jul. 2017, doi: 10.1016/J.OPTMAT.2017.04.009.

[8] R. Zhang, Y. Wang, M. Jia, J. Xu, and E. Pan, "One-pot hydrothermal synthesis of ZnS quantum dots/graphene hybrids as a dual anode for sodium ion and lithium ion batteries," *Appl Surf Sci*, vol. 437, pp. 375–383, Apr. 2018, doi: 10.1016/J.APSUSC.2017.12.110.

[9] T. I. Chanu, D. Samanta, A. Tiwari, and S. Chatterjee, "Effect of reaction parameters on photoluminescence and photocatalytic activity of zinc sulfide nanosphere synthesized by hydrothermal route," *Appl Surf Sci*, vol. 391, pp. 548–556, Jan. 2017, doi: 10.1016/J.APSUSC.2016.05.045.

[10] Komal, P. Shikha, and T. S. Kang, "Facile and green one pot synthesis of zinc sulphide quantum dots employing zinc-based ionic liquids and their photocatalytic activity," *New Journal of Chemistry*, vol. 41, no. 15, pp. 7407–7416, Jul. 2017, doi: 10.1039/C7NJ01373F.

[11] T. Kumar, Shreya, P. Phogat, V. Sahgal, and R. Jha, "Surfactant-mediated modulation of morphology and charge transfer dynamics in tungsten oxide nanoparticles," *Phys Scr*, vol. 98, no. 8, p. 085936, Jul. 2023, doi: 10.1088/1402-4896/ACE566.

[12] Dipti, P. Phogat, Shreya, D. Kumari, and S. Singh, "Fabrication of tunable band gap carbon based zinc nanocomposites for enhanced capacitive behaviour," *Phys Scr*, vol. 98, no. 9, p. 095030, Aug. 2023, doi: 10.1088/1402-4896/ACF07B.

[13] P. Phogat, Shreya, R. Jha, and S. Singh, "Diffusion Controlled Features of Microwave Assisted ZnS/ZnO Nanocomposite with Reduced Band Gap," *ECS Journal of Solid State Science and Technology*, vol. 12, no. 3, p. 034004, Mar. 2023, doi: 10.1149/2162-8777/ACC426.

[14] Shreya, P. Phogat, R. Jha, and S. Singh, "Microwave-synthesized γ-WO3 nanorods exhibiting high current density and diffusion characteristics," *Transition Metal Chemistry*, vol. 48, no. 3, pp. 167–183, Jun. 2023, doi: 10.1007/S11243-023-00533-Y/FIGURES/16.

[15] S. Sharma, P. Phogat, R. Jha, and S. Singh, "Electrochemical and Optical Properties of Microwave Assisted MoS2 Nanospheres for Solar Cell Application Electrochemical and Optical Properties of Microwave Assisted MoS 2 Nanospheres for Solar Cell Application," *Article in International Journal of Smart Grid and Clean Energy*, 2023, doi: 10.12720/sgce.12.3.66-72.

[16] P. Phogat, S. Shreya, R. Jha, and S. Singh, “Impedance Study of Zinc Sulphide Quantum Dots via One Step Green Synthesis,” *Materials Science Forum*, vol. 1099, pp. 119–125, Oct. 2023, doi: 10.4028/P-G1CCXQ.